Molecular Dissection of the Interface between the Type VI Secretion TssM Cytoplasmic Domain and the TssG Baseplate Component

Laureen Logger, Marie-Stéphanie Aschtgen, Marie Guérin, Eric Cascales and Eric Durand

Laboratoire d'Ingénierie des Systèmes Macromoléculaires, *Institut de Microbiologie de la Méditerranée, Aix-Marseille Université, CNRS – UMR 7255, 31 Chemin Joseph Aiguier, 13402 Marseille Cedex 20, France*

Correspondence to Eric Cascales and Eric Durand: *cascales@imm.cnrs.fr; edurand@imm.cnrs.fr*
http://dx.doi.org/10.1016/j.jmb.2016.08.032
Edited by Bert Poolman

Abstract

The type VI secretion system (T6SS) is a multiprotein complex that catalyses toxin secretion through the bacterial cell envelope of various Gram-negative bacteria including important human pathogens. This machine uses a bacteriophage-like contractile tail to puncture the prey cell and inject harmful toxins. The T6SS tail comprises an inner tube capped by the cell-puncturing spike and wrapped by the contractile sheath. This structure is built on an assembly platform, the baseplate, which is anchored to the bacterial cell envelope by the TssJLM membrane complex (MC). This MC serves as both a tail docking station and a channel for the passage of the inner tube. The TssM transmembrane protein is a key component of the MC as it connects the inner and outer membranes. In this study, we define the TssM topology, highlighting a large but poorly studied 35-kDa cytoplasmic domain, $TssM_{Cyto}$, located between two transmembrane segments. Protein–protein interaction assays further show that $TssM_{Cyto}$ oligomerises and makes contacts with several baseplate components. Using computer predictions, we delineate two subdomains in $TssM_{Cyto}$, including a nucleotide triphosphatase (NTPase) domain, followed by a 110-aa extension. Finally, site-directed mutagenesis coupled to functional assays reveals the contribution of these subdomains and conserved motifs to the interaction with T6SS partners and to the function of the secretion apparatus.

Introduction

The type VI secretion system (T6SS) is a versatile multiprotein secretory machine that is implicated in both interbacterial competition and anti-eukaryotic host activities. The T6SS delivers a broad arsenal of toxins with peptidoglycan, phospholipid, or DNA hydrolysis activities or induces cytoskeleton rearrangements directly into the target cell [1–4].

For toxin delivery, the T6SS uses a contractile mechanism that is comparable to that of *Myoviridae* phages or R-pyocins [5–10]. This machine is composed of 13 core subunits, categorised in three subcomplexes [8,10–12]: a cytoplasmic tubular structure built on an assembly platform—or baseplate (BP)—that is evolutionarily, structurally, and functionally related to bacteriophage contractile tails [5,13–15] and is anchored to the cell envelope by a membrane complex (MC) [16].

The T6SS tail is composed of an inner tube made of stacked Hcp hexameric rings and is wrapped into a sheath-like structure, formed by the polymerisation of TssB–TssC heterodimeric complexes and that is assembled in an extended conformation [14,17–19]. Indeed, the assembly of the tail can be followed by time-lapse microscopy: fluorescent-labelled sheath components assemble a ~600-nm-long tubular structure in tens of seconds, which then contracts in a few milliseconds [14,20]. The contraction of the sheath coincides with bacterial prey lysis, suggesting that similar to phages, sheath contraction propels the inner tube towards the target cell, allowing the delivery of toxin effectors [8,11,20,21]. The assembly of the tube and the sheath is coordinated by TssA, a protein that controls the elongation of the tail at the distal end and that maintains the sheath under the extended conformation [22]. The inner tube is tipped by a spike constituted of a trimer of the VgrG

Please cite this article as: L. Logger, et al., Molecular Dissection of the Interface between the Type VI Secretion TssM Cytoplasmic Domain and the TssG Baseplate Component, J. Mol. Biol. (2016), http://dx.doi.org/10.1016/j.jmb.2016.08.032

protein, which is proposed to puncture the target cell membrane [13,23]. The VgrG trimer is also part of the BP that is used as an assembly platform for the tail. Recently, the T6SS BP composition has been revealed. In addition to VgrG, it is composed of the TssE, -F, and -G subunits, the homologues of the phage T4 gp25, gp6, and gp7 proteins, respectively, and of TssK, a protein of unknown function with limited homologies to phage T4 gp8 or gp10 proteins that has been proposed to be a connector to the MC [15,24–27]. This MC is composed of the two TssL and TssM inner membrane (IM) proteins and of the TssJ outer membrane (OM) lipoprotein [28–32]. TssL and TssM interact in the IM, whereas the C-terminal periplasmic domain of TssM contacts the TssJ lipoprotein close to the OM [16,29,30,33–35]. The MC serves as a docking station for the BP and the tail but has also been proposed to serve as a channel for the passage of the inner tube during sheath contraction [16]. In the recent years, the assembly pathway of the T6SS has been well defined. T6SS biogenesis progresses from the OM to the cytoplasm. It starts with the positioning of the TssJ lipoprotein and the successive recruitments of TssM and TssL [16]. Recruitment of TssA then positions the BP complex onto the MC and primes the polymerisation of the tail tube/sheath [15,22,36]. This ordered assembly pathway requires tight contacts between the different subunits. Indeed, docking of the BP onto the MC requires multiple contacts including the interactions of TssE and TssK with TssL and of TssG and TssK with TssM [15,24]. TssM is therefore a key component as it mediates contact with the OM TssJ lipoprotein and with cytoplasmic BC subunits.

Here, we show that the enteroaggregative *Escherichia coli* (EAEC) TssM protein is a polytopic membrane protein, inserted into the IM by three transmembrane helices (TMH). The C-terminal portion of TssM is in the periplasm and interacts with TssJ [34]. TMH2 and TMH3 delimitates a ~35-kDa cytoplasmic domain, $TssM_{Cyto}$, which is conserved among TssM homologues. Computer analyses show that $TssM_{Cyto}$ is constituted of two subdomains: a subdomain with a nucleotide triphosphatase (NTPase)-like domain, followed by an extension. Indeed, TssM has been previously shown to bind and hydrolyse nucleotide triphosphates (NTPs) [37]. However, the role of the NTP-binding motif and its functional implication during T6SS activity are still a matter of debate [29,33]. The extension comprises a eukaryotic Dumpy-30 (DPY-30)-like dimerisation motif. We show that the NTPase-like domain mediates the interaction with TssK, whereas the extension is necessary and sufficient for $TssM_{Cyto}$ oligomerisation and interaction with TssG. Site-directed mutagenesis of conserved motifs within the extension revealed their contribution for $TssM_{Cyto}$ oligomerisation and $TssM_{Cyto}$–TssG interaction and for proper assembly of the T6SS. Our results thus provide details on the molecular interface between the T6SS membrane and the BP complexes.

Results

TssM is a polytopic IM protein

The TssM protein encoded within the EAEC *sci-1* gene cluster [EC042_4539; Genbank accession (GI): 284924260] is a large protein of 1129 aa. Based on hydrophobicity plots, the most widely used computer tools predict TssM as an IM protein with three TMH (Fig. 1a). Indeed, fractionation experiments showed that TssM co-fractionates with membrane proteins (data not shown). To experimentally define the TssM topology and determine the TMH boundaries, we performed a cysteine accessibility assay using the substituted cysteine accessibility method [38]. This assay relies on the ability of 3-(*N*-maleimidylpropionyl) biocytin (MPB), a sulfhydryl reagent, to cross the OM but not the IM of Gram-negative bacteria including EAEC [30,31]. TssM possesses nine native cysteine residues, with one (C727) predicted to locate in the periplasm. Hence, the wild-type (WT) TssM protein is labelled by MPB *in vivo* (Fig. 1b). In agreement with the computer predictions, a TssM protein, in which the cysteine at position 727 is substituted to serine (C727S), was not labelled with MPB (Fig. 1b). These data suggest that C727 is located in the periplasm, whereas all other eight cysteine residues are located in the cytoplasm or buried into the structure of the protein and are then inaccessible to MPB. We then introduced cysteine substitutions in the C727S TssM variant at various positions along the protein (at positions 37, 67, 352, and 386; Fig. 1a). All these mutated proteins were produced at similar levels (Fig. 1b) and were able to complement the effect of the *tssM* mutant in an Hcp secretion assay (data not shown). The A37C and S386C variants were biotinylated with MPB, suggesting that the A37 and S386 residues are located in the periplasm (Fig. 1b). By contrast, the V67C and S352C variants were not labelled, indicating that the V67 and S352 residues are located in the cytoplasm (Fig. 1b). Altogether, the data of the cysteine accessibility defined the topology of TssM; TssM is constituted of three TMH, with the N terminus in the cytoplasm and the C terminus in the periplasm. TssM spans the IM through two TMH-oriented in-to-out (TMH1, residues 13–29; TMH3, residues 360–382) and one TMH-oriented out-to-in (TMH2, residues 44–62; Fig. 1c). TMH2 and TMH3 thus delimitate a ~35-kDa domain located in the cytoplasm, called $TssM_{Cyto}$ hereafter.

The cytoplasmic domain of TssM oligomerises and interacts with the components of the T6SS membrane and BP complexes

The topology of TssM indicates the existence of two soluble domains, one in the periplasm ($TssM_{Peri}$,

Please cite this article as: L. Logger, et al., Molecular Dissection of the Interface between the Type VI Secretion TssM Cytoplasmic Domain and the TssG Baseplate Component, J. Mol. Biol. (2016), http://dx.doi.org/10.1016/j.jmb.2016.08.032

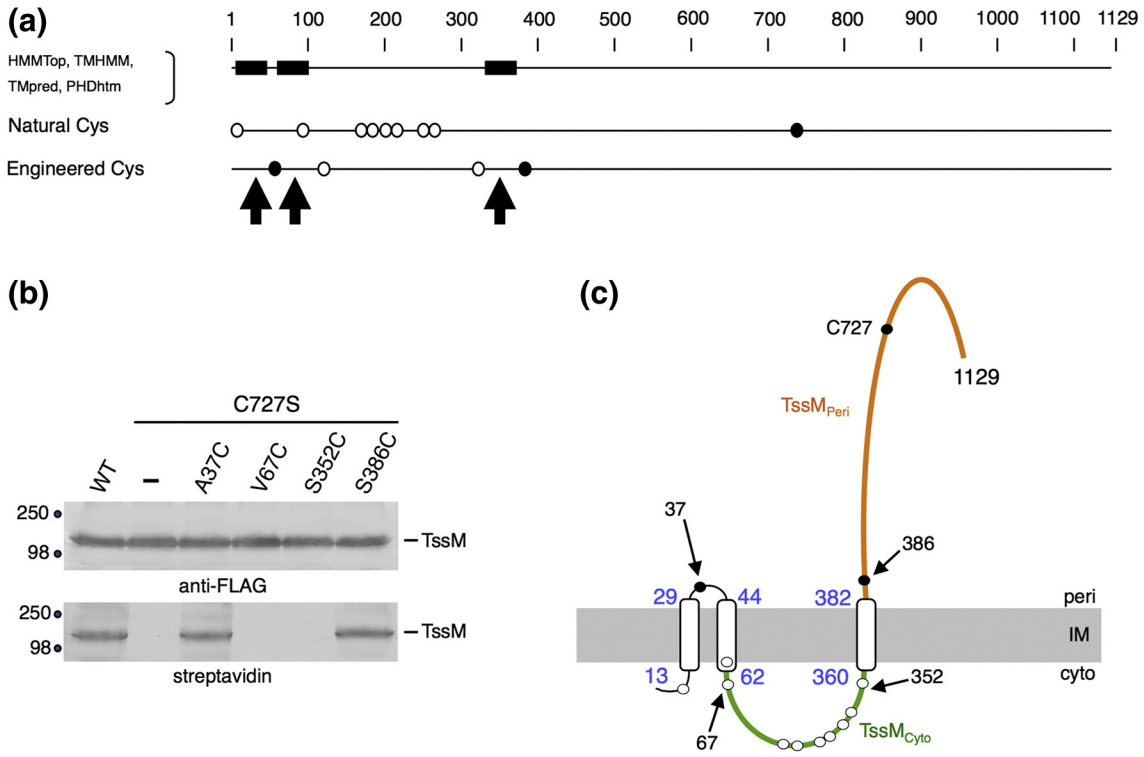

Fig. 1. TssM is a polytopic IM protein. (a) The transmembrane helices (TMH) predicted using the algorithms listed on the left are represented by black rectangles. The EAEC Sci-1 TssM natural cysteine residues and the cysteine substitutions engineered in this study are indicated. Filled circles indicate cysteine residues labelled with the 3-(*N*-maleimidylpropionyl) biocytin (MPB) probe, whereas open circles indicate unlabelled cysteine residues. Arrowheads indicate transmembrane segments determined experimentally. (b) Accessibility of cysteine residues. Whole EAEC Δ*tssM* cells producing WT TssM (WT) or the indicated mutant proteins were labelled with the MPB probe, lysed, and solubilised, and TssM and mutant proteins were immunoprecipitated with anti-FLAG-coupled beads. The precipitated material was subjected to SDS-PAGE and Western blot analysis using anti-FLAG antibody (TssM detection, upper panel) and streptavidin coupled to alkaline phosphatase (MPB-labelled TssM detection, lower panel). Molecular weight markers are indicated on the left. (c) Topology model for the EAEC TssM protein at the IM. The localisations of the labelled and unlabelled cysteine residues are indicated by filled and open circles, respectively. The cytoplasmic ($TssM_{Cyto}$) and periplasmic ($TssM_{Peri}$) domains are highlighted in green and orange, respectively. The three transmembrane segments identified by the accessibility studies are shown, with their membrane boundaries (in blue).

amino acids 383–1129) and one residing into the cytoplasm ($TssM_{Cyto}$, amino acids 63–359). The T6SS is a multiprotein complex in that the large protein domains might be necessary for interacting with other T6SS components. Indeed, we and others have previously demonstrated that $TssM_{Peri}$ interacts with the TssJ OM lipoprotein in *Edwardsiella tarda* and EAEC [33,34]. By contrast, little is known regarding the cytoplasmic domain of TssM. To gain further insights into $TssM_{Cyto}$ partners, we used $TssM_{Cyto}$ as a bait for an *in vivo* systematic, bacterial two-hybrid assay. $TssM_{Cyto}$ was fused to the T18 domain of the *Bordetella* adenylate cyclase, and all the other T6SS proteins—or soluble domains—were fused at their N or C terminus of the T25 domain. The results presented in Fig. 2 show that $TssM_{Cyto}$ interacts with itself and TssK whatever the constructions used. In addition, $TssM_{Cyto}$ interacts with TssG and the cytoplasmic domain of TssL ($TssL_{Cyto}$) when fused at the N terminus of T25. In conclusion, $TssM_{Cyto}$ is capable of oligomerisation and interacts with the components of the T6SS membrane ($TssL_{Cyto}$) and BP (TssK and TssG) complexes. These results are in agreement with the previously published bacterial two-hybrid screens and co-immunoprecipitations that identified TssM–TssK, TssM–TssL, and TssM–TssG interactions [15,24,29,30].

Subdomain architecture of $TssM_{Cyto}$

Pfam, Blast, and HHPred analyses suggest that EAEC $TssM_{Cyto}$ is organised as an NTPase domain ($TssM_{Cyto/NTP}$; amino acids 62–248; Pfam accession: PF06858), followed by a C-terminal extension ($TssM_{Cyto/Ct}$; amino acids 254–360; Fig. 3 and Supplementary Figs. S1 and S2). However, despite

Please cite this article as: L. Logger, et al., Molecular Dissection of the Interface between the Type VI Secretion TssM Cytoplasmic Domain and the TssG Baseplate Component, J. Mol. Biol. (2016), http://dx.doi.org/10.1016/j.jmb.2016.08.032

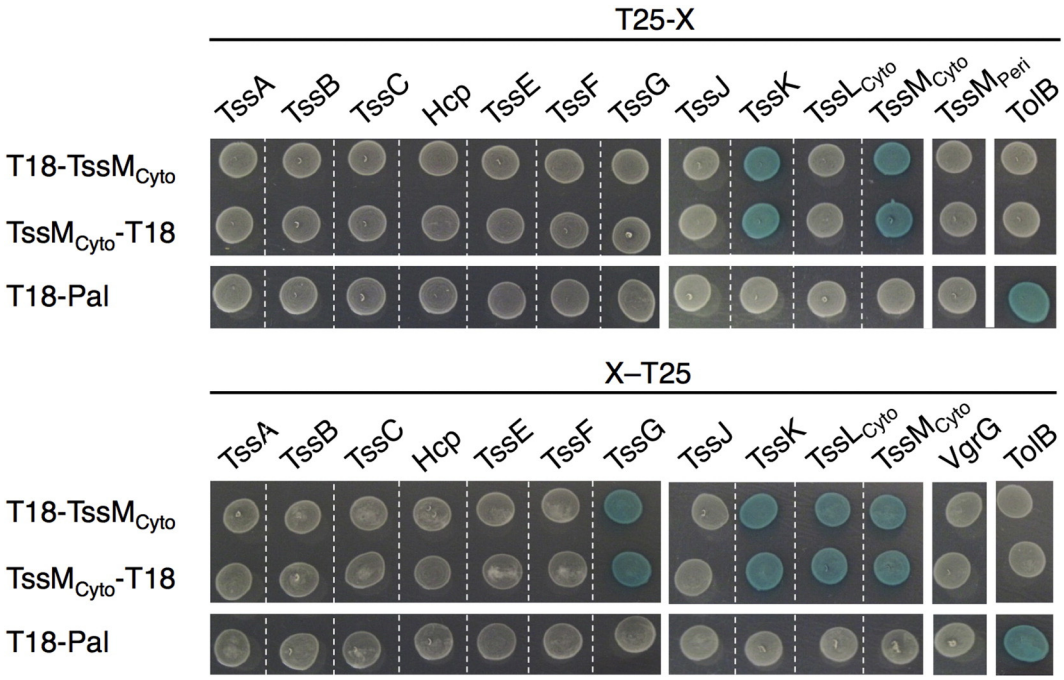

Fig. 2. $TssM_{Cyto}$ interaction network identified by bacterial two-hybrid analysis. BTH101 reporter cells carrying pairs of plasmids producing the indicated T6SS proteins fused to the T18 or T25 domain of the *Bordetella* adenylate cyclase were spotted on X-Gal-IPTG indicator LB agar plates. Only the cytoplasmic (Cyto) or periplasmic (Peri) domains were used for membrane-anchored proteins. Controls include T18 and T25 fusions to TolB and Pal, two proteins that interact but are unrelated to the T6SS.

the fact that the overall NTPase domain is conserved among the $TssM_{Cyto}$ homologues, the sequence alignment shows that the NTP-binding and hydrolysis motifs (Walkers A & B and NTP specific motif) are not well conserved (Supplementary Fig. S1). In agreement with this observation, an evolutionary analysis of $TssM_{Cyto}$ NTPase domains shows that they categorise into two subgroups: while the TssM proteins encoded within the *Pseudomonas aeruginosa* H1, *Agrobacterium tumefaciens*, and *E. tarda* T6SS gene clusters carry a complete NTPase domain, a number of TssM, including that of EAEC, *Serratia*, and *Citrobacter*, possess an NTPase domain amputated of hydrolysis motifs (Supplementary Figs. S1 and S2).

Our attempts to produce and purify the EAEC $TssM_{Cyto}$ domain or the $TssM_C$ NTPase subdomain in order to gain structural information were unsuccessful, as the different constructs used were all insoluble. Consequently, we sought to construct homology-based models of both $TssM_{Cyto}$ subdomains using a bioinformatic approach. The $TssM_{Cyto/NTP}$ structure was predicted using HHpred [39]. The program confirmed that the EAEC $TssM_{Cyto/NTP}$ protein resembles the solved structure of various Guanosine triphosphate (GTP)-hydrolysing proteins (Supplementary Fig. S3). The X-ray structure of the *Burkholderia thailandensis* EngB GTP-binding protein (PDB ID: 4DHE) [40] was subsequently used as template to build a homology model of the EAEC $TssM_{Cyto/NTP}$ domain. Figure 3 shows that $TssM_{Cyto/NTP}$ adopts a compact fold consisting of a four-stranded parallel β-sheet with one side being in contact with three α-helices. The $TssM_{Cyto/NTP}$ domain belongs to the α/β class, harbouring an incomplete Rossmann fold, a motif associated with nucleotide-binding proteins [41]. The EAEC $TssM_{Cyto/NTP}$ architecture is typical of P-loop NTP hydrolases. The predicted structure of EAEC $TssM_{Cyto/NTP}$ diverges, however, from the classical αβα sandwich architecture, as the second α-helix is not strictly sandwiching the β-strand. As expected, the large loops that bear the binding and hydrolysis motifs are absent in the EAEC $TssM_{Cyto/NTP}$, by contrast to EngB or the homology model of the *A. tumefaciens* $TssM_{Cyto/NTP}$ domain (Supplementary Fig. S4). The $TssM_{Cyto/Ct}$ homology model was constructed using the Swiss-Model server based on the X-ray structure of the C-terminal domain of human DPY-30-like protein, a component of the eukaryotic histone methyltransferase complex (PDB ID: 3G36) [42], as template (Supplementary Fig. S3). The $TssM_{Cyto/Ct}$ structure was confidently modelled from residue Q254 to N289 (Fig. 3). This fragment encompasses the two-helix 40-aa DPY-30 motif (Pfam accession: PF05186) found in DPY-30 proteins and is involved in DPY-30 dimerisation [42].

Please cite this article as: L. Logger, et al., Molecular Dissection of the Interface between the Type VI Secretion TssM Cytoplasmic Domain and the TssG Baseplate Component, J. Mol. Biol. (2016), http://dx.doi.org/10.1016/j.jmb.2016.08.032

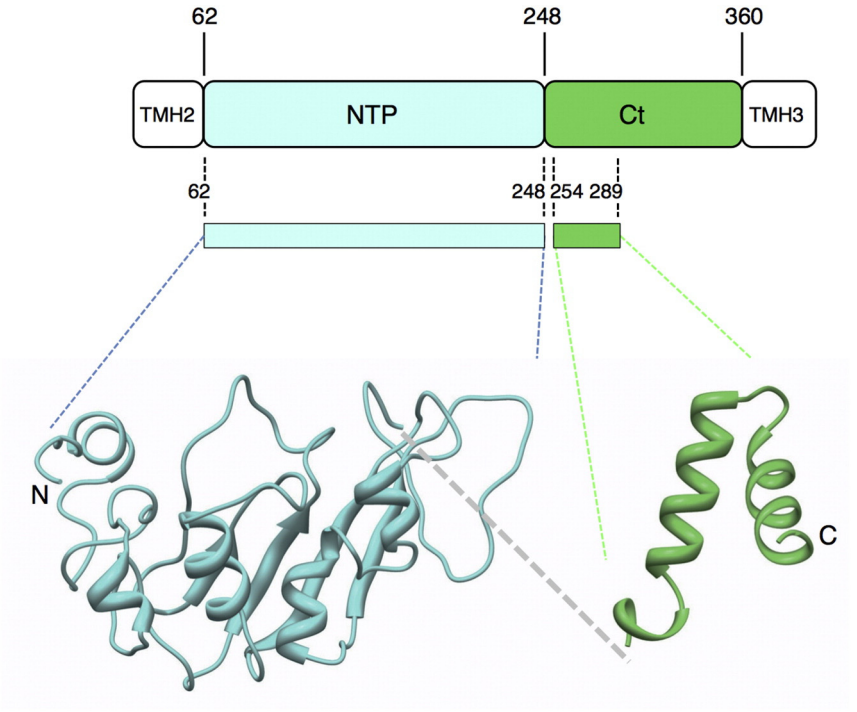

Fig. 3. Structural architecture of $TssM_{Cyto}$. (a) The cytoplasmic domain of TssM and $TssM_{Cyto}$, delimitated by the TMH2 and TMH3 could be partitioned into an NTPase-like domain (NTP, blue) and a C-terminal extension (Ct, green). $TssM_{Cyto/NTP}$ was modelled using HHpred based on the X-ray structure of the *Burkholderia thailandensis* EngB GTP-binding protein (PDB ID: 4DHE). $TssM_{Cyto/Ct}$ was modelled using SwissModel based on the X-ray structure of the C-terminal domain of the human DPY-30-like protein, a component of the histone methyltransferase complex (PDB ID: 3G36). All images were made with Chimera [66].

Specific motifs are involved in $TssM_{Cyto}$ oligomerisation and interaction with TssG

The structural organisation of $TssM_{Cyto}$ prompted us to investigate the contribution of the two subdomains to the $TssM_{Cyto}$ interactions. The interaction network of $TssM_{Cyto/NTP}$ and $TssM_{Cyto/Ct}$ was assessed by bacterial two-hybrid. As shown in Fig. 4a, $TssM_{Cyto/NTP}$ interacts with TssK, whereas $TssM_{Cyto/Ct}$ mediates oligomerisation and interactions with TssG and $TssL_{Cyto}$. Interestingly, the interaction network of the isolated subdomains, $TssM_{Cyto/NTP}$ and $TssM_{Cyto/Ct}$, recapitulates the interaction network of $TssM_{Cyto}$ (Fig. 4a), supporting the hypothesis of two independently folded domains. The $TssM_{Cyto/Ct}$–TssG and $TssM_{Cyto/NTP}$–TssK interactions were further confirmed by co-immunoprecipitation experiments; TssG was co-precipitated with $TssM_{Cyto}$ and $TssM_{Cyto/Ct}$ (Fig. 4b, upper panel). As previously shown [24], TssK did not interact with $TssM_{Cyto}$ by co-immunoprecipitation. However, our results suggest that it is prevented by the extension, as the $TssM_{Cyto/NTP}$ domain alone interacts with TssK (Fig. 4B, lower panel).

Interestingly, the $TssM_{Cyto/Ct}$ subdomain interacts with several partners from the membrane and BP subcomplexes. We therefore questioned whether these different interactions involve the same recognition motif or different binding epitopes on $TssM_{Cyto}$. The sequence alignment of $TssM_{Cyto}$ homologues emphasised two well-conserved regions, F278-E284 and L309-S315 (Supplementary Fig. S1). Region F278-E294 is specifically conserved in $TssM_{Cyto}$ lacking functional NTPase domain, whereas the L309-S315 motif is conserved among all $TssM_{Cyto}$ (Supplementary Fig. S1). Using site-directed mutagenesis, we engineered $TssM_{Cyto}$ variants in which these motifs were targeted. Although these two motifs do not appear to be involved in $TssM_{Cyto}$–$TssL_{Cyto}$ interactions, substitutions within the L309-S315 motif specifically abolished the $TssM_{Cyto}$–TssG interaction (Fig. 5a and B). We also noted that the substitutions within the F278-E284 motif impacted $TssM_{Cyto}$ oligomerisation. However, although the L279W and L282W/A283W mutations prevented the interaction with $TssM_{Cyto}$ in the bacterial two-hybrid assay (Fig. 5a), only the L279W mutations had a strong effect on multimerisation in the co-immunoprecipitation assay (Fig. 5b). It is worthy to note that the $TssM_{Cyto/Ct}$ F278-E284 residues correspond to the dimerisation motif in DPY-30 proteins (Supplementary Fig. S4B).

$TssM_{Cyto}$ oligomerisation and interaction with the TssG BP subunit are critical for T6SS function

The mutations that specifically affect $TssM_{Cyto}$ oligomerisation and $TssM_{Cyto}$–TssG complex formation were tested for their repercussion on T6SS function. EAEC Sci-1 T6SS function could be monitored by measuring its antibacterial activity [43]. The four TssM substitutions were introduced within the native, chromosomal *tssM* gene. Figure 6a shows that all four mutated strains were defective in T6SS-dependent killing of prey bacterial cells. We therefore conclude that $TssM_{Cyto}$ oligomerisation and interaction with TssG are required for the proper function of the type VI secretion apparatus.

Please cite this article as: L. Logger, et al., Molecular Dissection of the Interface between the Type VI Secretion TssM Cytoplasmic Domain and the TssG Baseplate Component, J. Mol. Biol. (2016), http://dx.doi.org/10.1016/j.jmb.2016.08.032

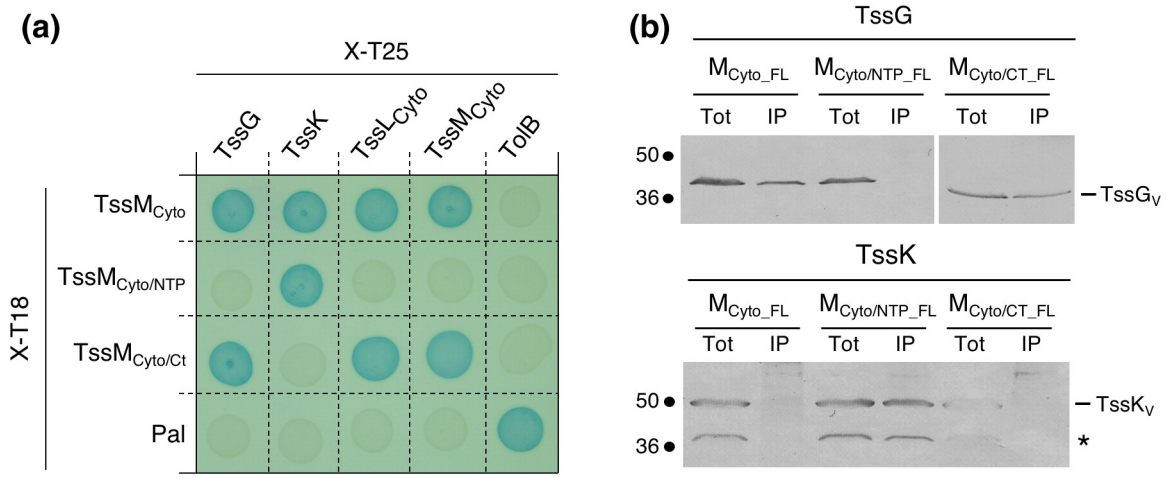

Fig. 4. The two TssM$_{Cyto}$ subdomains mediate the interaction with two BP components. (a) Bacterial two-hybrid assay. BTH101 reporter cells carrying pairs of plasmids producing the indicated T6SS proteins fused to the T18 or T25 domain of the *Bordetella* adenylate cyclase were spotted on X-Gal-IPTG indicator LB agar plates. Only the cytoplasmic ($_C$) or periplasmic ($_P$) domains were used for membrane-anchored proteins. Controls include T18 and T25 fusions to TolB and Pal, two proteins that interact but are unrelated to the T6SS. (b) Co-immunoprecipitation assay. Soluble lysates from 5×10^{10} *E. coli* K12 W3110 cells producing FLAG-tagged TssM$_{Cyto}$ (M$_{Cyto_FL}$), FLAG-tagged TssM$_{Cyto/NTP}$ (NTP$_{FL}$) or FLAG-tagged TssM$_{Cyto/Ct}$ (Ct$_{FL}$), and VSV-G-tagged TssG (TssG$_V$) or TssK (TssK$_V$) proteins were subjected to immunoprecipitation with anti-FLAG-coupled beads. The total soluble (Tot) and the immunoprecipitated (IP) material were separated by 12.5% acrylamide SDS-PAGE and immunodetected with anti-VSVG (TssG$_V$ or TssK$_V$) monoclonal antibodies. Molecular weight markers (in kDa) are indicated on the left. The asterisk on the lower panel indicates a degradation product from the TssK protein.

T6SS biogenesis starts with the assembly of the MC and is followed by (i) the recruitment of the BP and (ii) tail polymerisation. We therefore sought to define which stage of T6SS biogenesis is impacted by these mutations. We first tested the effects of these mutations on T6SS sheath assembly by following the

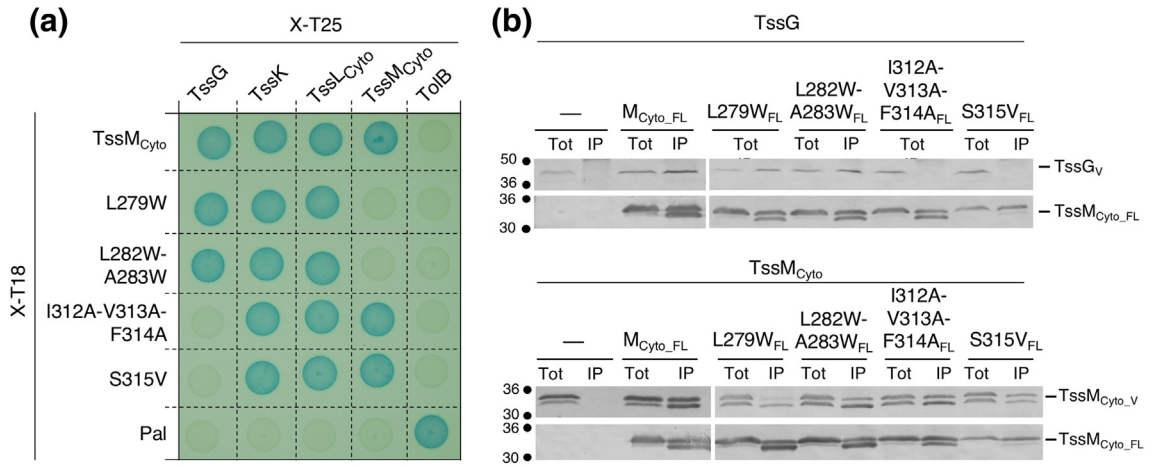

Fig. 5. Specific conserved motifs mediate TssM$_{Cyto}$ dimerisation and interaction with TssG. (a) Bacterial two-hybrid assay. BTH101 reporter cells carrying pairs of plasmids producing the indicated T6SS proteins fused to the T18 or T25 domain of the *Bordetella* adenylate cyclase were spotted on X-Gal-IPTG indicator LB agar plates. Only the cytoplasmic ($_C$) or periplasmic ($_P$) domains were used for membrane-anchored proteins. Controls include T18 and T25 fusions to TolB and Pal, two proteins that interact but are unrelated to the T6SS. (b) Co-immunoprecipitation assay. Soluble lysates from 5×10^{10} *E. coli* K12 W3110 cells producing FLAG-tagged TssM$_C$ WT (M$_{Cyto_FL}$) or mutants and VSV-G-tagged TssG (TssG$_V$) or TssM$_{Cyto}$ (TssM$_{Cyto_V}$) proteins were subjected to immunoprecipitation with anti-FLAG-coupled beads. The total soluble (Tot) and the immunoprecipitated (IP) material were separated by 12.5% acrylamide SDS-PAGE and immunodetected with anti-FLAG (lower panels) and anti-VSV-G (upper panels) monoclonal antibodies. Molecular weight markers (in kDa) are indicated on the left.

Please cite this article as: L. Logger, et al., Molecular Dissection of the Interface between the Type VI Secretion TssM Cytoplasmic Domain and the TssG Baseplate Component, J. Mol. Biol. (2016), http://dx.doi.org/10.1016/j.jmb.2016.08.032

dynamics of a chromosomally encoded TssB-sfGFP fusion using fluorescence microscopy (Fig. 6b). All the substitutions severely affected T6SS sheath assembly as indicated by the decrease in the number of sheath per bacterial cell (Fig. 6b). While ~25% of the WT cells assembled sheath structures, the TssBC sheath assembled on rare occasions in cells carrying mutations affecting $TssM_{Cyto}$ oligomerisation (3–4% of cells with sheath structures). The effect of the $TssM_{Cyto}$–TssG disruption was even more drastic, as sheath assembly was observed in ~1% of the cells.

Second, we tested the effect of these mutations on the recruitment of the BP. By following the dynamics of a sfGFP–TssF fusion, a recent study concluded that the MC recruits and stabilises the T6SS BP [15]. We therefore investigated whether the mutations affecting the oligomerisation of the cytoplasmic loop of TssM and the contacts between this loop and the TssG BP component impact BP assembly, stability, and recruitment. As TssG-to-sfGFP fusions were previously shown to be nonfunctional [15], we introduced the TssM point mutations in a strain producing the chromosomal and functional sfGFP–TssF fusion, which is a TssG protein partner, and we monitored the formation and stability of BP foci by fluorescence microscopy (Fig. 6c). All four mutations significantly decreased the number of cells with sfGFP–TssF foci

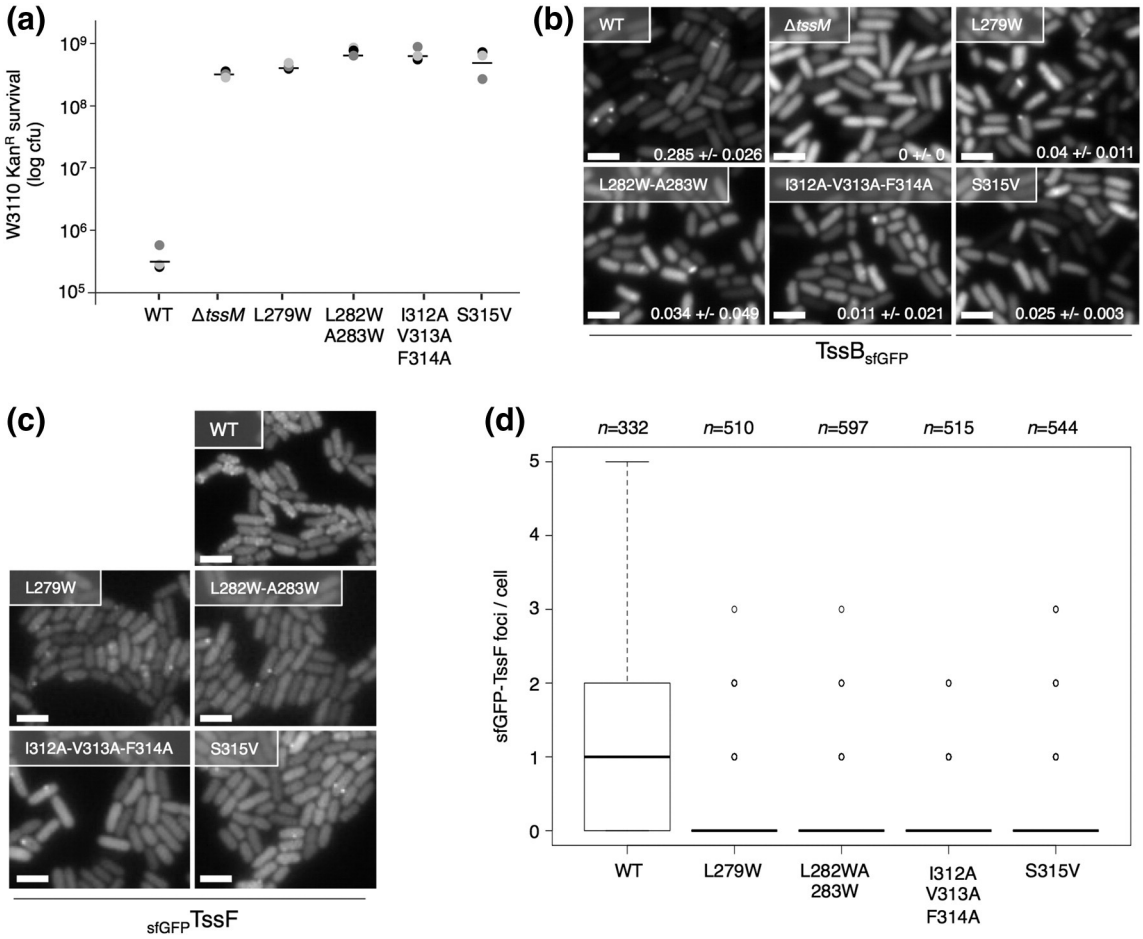

Fig. 6. $TssM_{Cyto}$ oligomerisation and interaction with the TssG BP are essential for T6SS function, sheath assembly, and BP stability. (a) Antibacterial assay. *E. coli* K-12 prey cells (W3110 *gfp*$^+$, kan^R) were mixed with the indicated attacker cells, spotted onto SIM agar plates, and incubated for 4 h at 37 °C. The number of recovered *E. coli* prey cells is indicated in the graph (in log10 of colony-forming unit). The circles indicate values from three independent assays, and the average is indicated by the bar. (b) Image recordings of the TssB-sfGFP fusion protein in the indicated cells. Statistical analyses (*n* = number of sheath/cell) are indicated under each strain. The number of cells studied per strain (*n*) is 150. The scale bar represents 2 μm. (c) Image recordings of the super folder Green Fluorescent Protein (sfGFP)–TssF fusion protein in the indicated cells. The scale bar represents 2 μm. (d) Statistical analyses of sfGFP–TssF in the indicated strains. Shown are box-and-whisker plots of the measured number of sfGFP–TssF foci per cell for each strain with the lower and upper boundaries of the boxes corresponding the 25% and 75% percentiles, respectively. The black bold horizontal bar represents the median values for each strain, and the whiskers represent the 10% and 90% percentiles. Outliers are shown as an open circle. *n* indicates the number of cells analysed per strain.

Please cite this article as: L. Logger, et al., Molecular Dissection of the Interface between the Type VI Secretion TssM Cytoplasmic Domain and the TssG Baseplate Component, J. Mol. Biol. (2016), http://dx.doi.org/10.1016/j.jmb.2016.08.032

and the average number of foci per cell (1 cluster in 15–25% of the mutated cells compared to 1–3 foci in ~65% for WT cells; Fig. 6c and d). Taken together, these data demonstrate that the mutations that affect $TssM_{Cyto}$ oligomerisation and $TssM_{Cyto}$–TssG complex formation abolish T6SS sheath formation and function by impacting T6SS BP assembly and stability.

Discussion

In this manuscript, we report the characterisation of the cytoplasmic domain of the T6SS membrane core complex protein TssM from EAEC. We showed that $TssM_{Cyto}$ comprises two subdomains, a domain resembling NTPases but lacking nucleotide-binding and hydrolysis motifs, followed by a ~110-aa extension. Protein–protein interaction studies revealed that this extension mediates $TssM_{Cyto}$ oligomerisation and interaction with the TssG BP subunit. We finally defined the specific motifs involved in these interactions and reported that these interactions are critical for the assembly of a functional T6SS. Models summarizing the findings reported in this study are depicted in Fig. 7.

We first defined the boundaries of the TssM transmembrane segments using cysteine accessibility experiments. We determined that TssM is constituted of three TMH. The TssM N terminus locates in the cytoplasm and is followed by a transmembrane hairpin, a cytoplasmic domain, and the third TMH, TMH3. Finally, the ~750-aa C-terminal domain locates in the periplasm (Fig. 1c). This topology is similar to the topology of the *A. tumefaciens* TssM protein previously defined using translational reporter fusions [29]. Computer analyses of TssM proteins encoded within well-studied T6SS gene cluster showed that this topology is likely shared among all the homologues with the notable exception of the *P. aeruginosa* H1-T6SS TssM protein that is predicted to have a single TMH corresponding to TMH3 (Supplementary Fig. S5).

The topology experiments also defined that TssM TMH2 and TMH3 delimit a 35-kDa cytoplasmic domain, $TssM_{Cyto}$. Our data showed that $TssM_{Cyto}$ oligomerises and interacts with $TssL_{Cyto}$. The $TssM_{Cyto}$–$TssM_{Cyto}$ and $TssM_{Cyto}$–$TssL_{Cyto}$ interactions have been reported in the *A. tumefaciens* T6SS [29]. The conservation of $TssM_{Cyto}$ oligomerisation and the interaction with $TssL_{Cyto}$ between *A. tumefaciens* and EAEC suggest that these contacts are important for T6SS function. Indeed, mutation of L279, a residue that participates to $TssM_{Cyto}$ oligomerisation, severely impacts T6SS function in EAEC. The low resolution of the recently

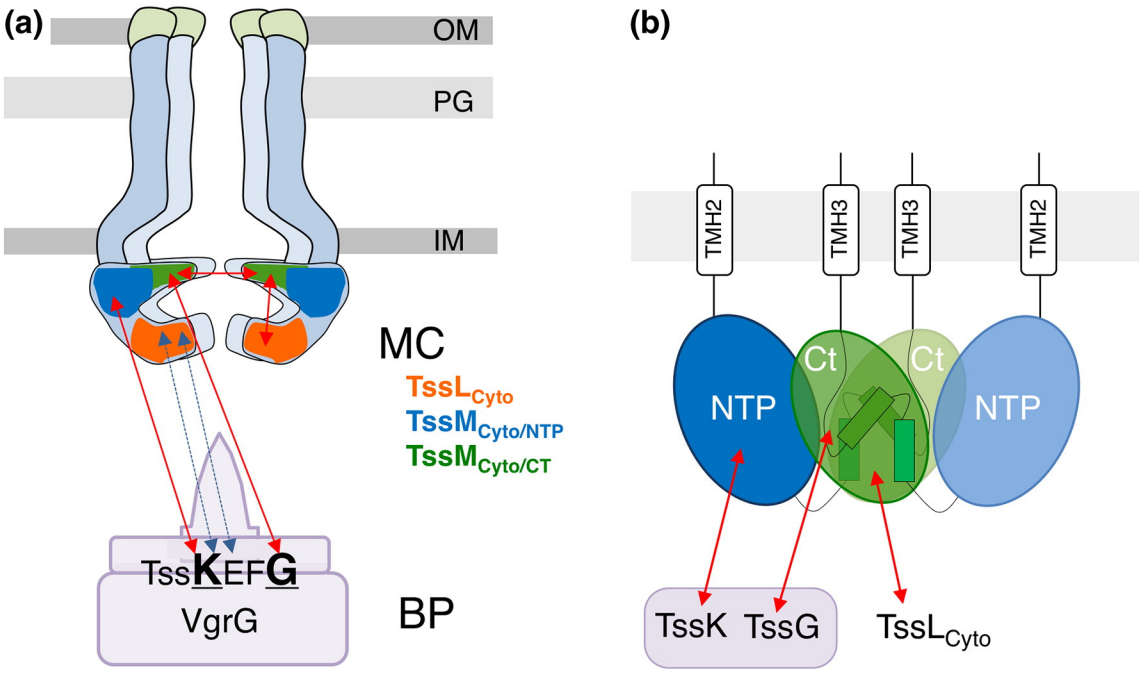

Fig. 7. Schematic representation of the $TssM_{Cyto}$ interaction network. (a) Schematic representation of the TssJLM MC and its interactions with the TssKEFG–VgrG BP complex. The $TssM_{Cyto/NTP}$ and $TssM_{Cyto/Ct}$ and the TssL cytoplasmic domain ($TssL_{Cyto}$) are shown in blue, green, and orange, respectively. The interactions defined in this study are indicated by red arrows. Interactions determined previously [24] or in the accompanying article [69] are shown in blue dashed arrows. (b) Schematic representation of a $TssM_{Cyto}$ dimer ($TssM_{Cyto/NTP}$ are shown in blue; $TssM_{Cyto/Ct}$ are shown in green). The cartoon highlights the $TssM_{Cyto/Ct}$–$TssM_{Cyto/Ct}$ interface and the interaction with TssK, TssG, and the cytoplasmic domain of TssL.

Please cite this article as: L. Logger, et al., Molecular Dissection of the Interface between the Type VI Secretion TssM Cytoplasmic Domain and the TssG Baseplate Component, J. Mol. Biol. (2016), http://dx.doi.org/10.1016/j.jmb.2016.08.032

published electron microscopy map of the 5-fold symmetry TssJLM MC does not allow the of use docking simulations to precisely locate the TssM cytoplasmic domain and therefore provide insight onto its oligomeric state in the complex. However, stoichiometry analyses and reconstruction of the MC suggested that it is constituted of five dimers of the TssJLM heterotrimers [16]. These information suggest that, similar to the TssL cytoplasmic domain [32], $TssM_{Cyto}$ dimerises. The biogenesis of the MC may therefore start with the formation of dimers of the heterotrimers that will then symmetrise. Based on the $TssM_{Cyto}$ interaction with the TssL cytoplasmic domain, it has been proposed that these two domains form the large base of the T6SS MC [16]. This cytoplasmic base corresponds to the docking site for the TssEFGK–VgrG BP complex [15,16,22]. Indeed, our bacterial two-hybrid and co-immunoprecipitation experiments confirmed that $TssM_{Cyto}$ interacts with two BP components, TssK and TssG (Fig. 7).

Bioinformatic analyses predict that $TssM_{Cyto}$ comprises an N-terminal NTPase domain and a C-terminal DPY-30-like domain named $TssM_{Cyto/NTP}$ and $TssM_{Cyto/Ct}$, respectively. However, although the EAEC $TssM_{Cyto/NTP}$ domain belongs to the NTPase fold, it misses the specific binding and hydrolysis motifs found in functional NTPases, such as the Walker A and B motifs. Sequence alignment of $TssM_{Cyto/NTP}$ domains from various bacterial species revealed that they categorise in two subfamilies. While a number of $TssM_{Cyto/NTP}$ domains do not carry these motifs, other TssM possess Walker A and B signatures, including that of *A. tumefaciens*, *E. tarda*, or *P. aeruginosa* H1-T6SS (Supplementary Fig. S2). Indeed, the detergent-solubilised *A. tumefaciens* TssM protein exhibits ATPase activity [37]. However, mutations of these motifs in *A. tumefaciens* and *E. tarda* did not have the same impact on the function of the T6SS. Production of the K124A TssM variant in *Edwardsiella* was fully functional as shown by T6SS-dependent Hcp, VgrG, and EvpP release [33]. By contrast, ATP binding and hydrolysis regulate conformational changes within the periplasmic domain of the *A. tumefaciens* TssM protein, and the *Agrobacterium* TssM K145A variant is unable to restore Hcp release [29,37]. Therefore, $TssM_{Cyto/NTP}$ domains come in different flavours: active NTPase domains (e.g., *A. tumefaciens*), inactive NTPase domains (e.g., *E. tarda*), and NTPase fold lacking the functional motifs (e.g., EAEC). Interestingly, our protein–protein interaction studies showed that $TssM_{Cyto/NTP}$ contacts TssK. In the case of TssM with functional NTP domains, it would be interesting to test whether the presence of TssK influences NTP binding and hydrolysis.

The $TssM_{Cyto}$ C-terminal extension shares structural homologies with the dimerisation motif of DPY-30, a subunit of the histone methyltransferase complex in eukaryotic cells. This two-α-helix motif forms an antiparallel bundle at the dimer interface, which is mediated by extensive hydrophobic and van der Waals interactions (Supplementary Fig. S4) [42]. Indeed, this DPY-30-like hairpin and, notably, the conserved L279 residues are involved in $TssM_{Cyto}$ oligomerisation. In addition to its role in $TssM_{Cyto}$ oligomerisation, this subdomain is also required for proper interaction with the cytoplasmic domain of TssL and $TssL_{Cyto}$ and with TssG, one of the components of the T6SS BP (Fig. 7). Whereas we have not identified in this study the residues of $TssM_{Cyto/Ct}$ mediating the interaction with $TssL_{Cyto}$, a conserved hydrophobic sequence (L-A-G-I-V-F-S in EAEC) is required for $TssM_{Cyto}$–TssG complex formation. Taken together, our results show that this relatively small subdomain is responsible for several interactions. Interestingly, a similar case has been reported for DPY-30, which is a partner of several complexes involved in the regulation of chromatin and nucleosome organisation [44]. One may hypothesise that $TssM_{Cyto/Ct}$ uses its DPY-30-like domain to interact sequentially with its different protein partners. Purification of the $TssM_{Cyto}$–$TssL_{Cyto}$–TssG complex or the high-resolution structure of the different binary complexes involving $TssM_{Cyto/Ct}$ will shed light on the dynamic nature of these interactions.

The interactions between $TssM_{Cyto}$ and TssK and TssG, the two components of the BP complex, might be important to recruit or stabilise the BC at the cytoplasmic base of the TssJLM MC. In addition to this structural role, it is likely that these interactions are required for proper function of the BP. As shown for other contractile structures such as bacteriophages, the BP serves as an assembly platform for the tail but is also responsible for initiating sheath contraction [26,45–47]. The $TssM_{Cyto}$–TssG interaction might therefore be important to regulate BP assembly, recruitment or sheath assembly, and/or contraction. Indeed, point mutations disrupting the $TssM_{Cyto}$–TssG interaction destabilise the BP complex and prevent the elongation of the tail sheath. It is interesting to note that TssM undergoes structural transitions [37], and one may suggest that TssM conformational changes might be transduced to the BP *via* the $TssM_{Cyto/NTP}$–TssK and/or $TssM_{Cyto/Ct}$–TssG interactions leading to sheath assembly. As TssM has a large periplasmic domain and a short extension that lies outside of the cell [16], it is a strong candidate to sense the modifications of the cell envelope, such as an attack by neighbouring cells or a contact with a prey, and to transmit the information to the BP complex. Further experiments will provide insights on how sheath assembly and/or contraction are regulated.

Our results also pointed that mutations disrupting $TssM_{Cyto}$ oligomerisation and $TssM_{Cyto}$–TssG complex formation affect T6SS-dependent activities, as they abolish TssBC sheath assembly and inhibit

Please cite this article as: L. Logger, et al., Molecular Dissection of the Interface between the Type VI Secretion TssM Cytoplasmic Domain and the TssG Baseplate Component, J. Mol. Biol. (2016), http://dx.doi.org/10.1016/j.jmb.2016.08.032

bacterial prey killing. The drastic effect of these mutations makes these interactions attractive targets for the rationale design of drugs that, by binding to $TssM_{Cyto}$, would hamper the T6SS activity and the delivery of harmful toxins. This approach has been successfully achieved in the case of the *Brucella* type IV secretion VirB8 IM subunit for which specific inhibitors of its dimerisation were identified by a high-throughput bacterial two-hybrid screen and were further shown to inhibit *Brucella* infection of macrophages [48,49]. This example emphasises the importance of understanding protein–protein interactions in bacterial secretion systems with the ultimate goal of targeting specific interactions with small-molecule inhibitors.

Materials and Methods

Bacterial strains, media, growth conditions, and chemicals

Strains used in this study are listed in Supplementary Table S1. *E. coli* K-12 DH5α, BTH101, and W3110 were used for cloning procedures, bacterial two-hybrid, and co-immunoprecipitation, respectively. The *E. coli* K-12 W3110 strain carrying the pUA66-*rrnB* plasmid (*gfp* under the control of the constitutive *rrnB* ribosomal promoter specifying strong and constitutive fluorescence and kanamycin resistance) [50] was used as prey in antibacterial competition experiments. EAEC strain 17-2 and its Δ*tssM*, *tssB-GFP*, and *GFP-tssF* derivatives [15,24,30] were used in this study. Chromosomal fluorescent reporter insertions were obtained using the modified one-step inactivation procedure [51] using the red recombinase expressed from pKOBEG [52], as previously described [28], using p*gfp*-KD4 as a template for PCR amplification. Briefly, the sfGFP-coding sequence and the kanamycin cassette were amplified from the p*gfp*-KD4 vector [15] with oligonucleotides carrying 50-nt extensions homologous to regions that are adjacent to the site of insertion. The PCR product was column purified (PCR and Gel Clean up kit, Promega) and electroporated. Kanamycin-resistant clones were recovered, and the insertion of the kanamycin cassette at the targeted site was verified by PCR. Kanamycin cassettes were then excised using pCP20 [51]. *tssM* point mutations were engineered at the native locus on the chromosome by allelic replacement using the pKO3 suicide vector [53,54]. Briefly, 17-2 *tssB-GFP* or *GFP-tssF* cells were transformed with a pKO3 plasmid in which a fragment of the *tssM* gene carrying the point mutations has been cloned (see below). Insertion of the plasmid into the chromosome was selected on chloramphenicol plates at 42 °C. Plasmid sequence removal was then selected on 5% sucrose plates without antibiotic, and *tssM* point mutation recombinant strains were screened by PCR and confirmed by DNA sequencing (Eurofins, MWG). Unless specified, cells were grown in LB or in *sci-1*-inducing medium (SIM; M9 minimal medium, 0.2% glycerol, 1 μg/mL vitamin B1, 100 μg/mL casaminoacids, and 10% LB, supplemented with or without 1.5% bactoagar) [55] at 37 °C with shaking. Plasmids were maintained by the addition of ampicillin (100 μg/mL), kanamycin (50 μg/mL), or chloramphenicol (30 μg/mL). Gene expression from pASK-IBA37+ and pBAD vectors was induced by the addition 0.1 μg/mL of anhydrotetracyclin (AHT; IBA Technology) and 0.02% of L-arabinose (Sigma-Aldrich), respectively.

Plasmid construction

Plasmids used in this study are listed in Supplementary Table S1. PCRs were performed using a Biometra thermocycler using the Q5 high-fidelity DNA polymerase (New England Biolabs). Restriction enzymes were purchased from New England Biolabs and used according to the manufacturer's instructions. Custom oligonucleotides, listed in Supplementary Table S1, were synthesised by Sigma-Aldrich. EAEC 17-2 chromosomal DNA was used as a template for all PCRs. *E. coli* strain DH5α was used for cloning procedures. With the exception of the pKO3-′*tssM*′ vector, plasmids have been constructed by restriction-free cloning [56] as previously described [30]. Briefly, genes of interest were amplified with oligonucleotides introducing the extensions annealing to the target vector. The double-stranded product of the first PCR has then been used as oligonucleotides for a second PCR using the target vector as a template. pKO3-′*tssM*′ has been constructed by the restriction–ligation procedure. A *Bam*HI-*Sal*I PCR product corresponding to a fragment of the *tssM* gene (nucleotides 216–1569) was ligated into pKO3 digested by the same enzymes using T4 DNA ligase (New England Biolabs). Substitutions into pIBA37-$_{FLAG}$TssM, pTssM$_{Cyto}$-T18, pT18-TssM$_{Cyto}$, and pKO3-′*tssM*′ have been introduced by site-directed mutagenesis using complementary pairs of oligonucleotides and the Pfu Turbo high-fidelity polymerase (Agilent Techologies). All constructs have been verified by restriction analysis and DNA sequencing (Eurofins, MWG).

Antibacterial assay

The antibacterial competition growth assay was performed as described [43]. The WT *E. coli* strain W3110 bearing the green fluorescent kanamycin-resistant pUA66-*rrnB* plasmid [50] was used as prey in the competition assay. The kanamycin-resistant pUA66-*rrnB* plasmid provides a strong constitutive green fluorescent phenotype. Attacker and prey cells were grown for 16 h in SIM and then diluted 100-fold in SIM. Once the culture reached an OD_{600} of 0.8, cells were harvested and resuspended to an OD_{600nm} of 10 in SIM. Attacker and prey cells were mixed to a 4:1 ratio, and 20-μL drops of the mixture were spotted in triplicate onto a prewarmed dry SIM agar plate. After incubation for 4 h at 37 °C, the bacterial spots were resuspended in LB, and bacterial suspensions were normalised to an OD_{600} of 0.5. For the enumeration of viable prey cells, bacterial suspensions were serially diluted and spotted onto selective LB agar plates supplemented with kanamycin (for the *E. coli* prey cells). The experiments were done in triplicate, with identical results, and we report here the results of a representative experiment.

Substituted cysteine accessibility method

Cysteine accessibility experiments were carried out as described [57,58] with modifications [30,31]. A 40-mL

Please cite this article as: L. Logger, et al., Molecular Dissection of the Interface between the Type VI Secretion TssM Cytoplasmic Domain and the TssG Baseplate Component, J. Mol. Biol. (2016), http://dx.doi.org/10.1016/j.jmb.2016.08.032

culture of strain Δ*tssM* producing the TssM or cysteine-substituted TssM derivatives was induced for *tssM* gene expression with 0.02% AHT for 2 h. Cells were harvested and then resuspended in buffer A [100 mM Hepes (pH 7.5), 250 mM sucrose, 25 mM $MgCl_2$, and 0.1 mM KCl] to a final OD_{600} of 12 in 500 μL of buffer A. MPB (Molecular Probes) was added to a final concentration of 100 μM (from a 20-mM stock freshly dissolved in Diméthylsulfoxyde (DMSO)), and the cells were incubated for 30 min at 25 °C. β-Mercaptoethanol (20 mM final concentration) was added to quench the biotinylation reaction, and cells were washed twice in buffer A and resuspended in buffer A containing *N*-ethylmaleimide (5 mM final concentration) to block all free sulfhydryl residues. After incubation for 20 min at 25 °C, cells were disrupted by four passages at the French press at 800 psi. Membranes recovered by ultracentrifugation for 40 min at 100,000*g* were resuspended in 1 mL of buffer B [10 mM Tris (pH 8.0), 100 mM NaCl, 1% (wt/vol) Triton X-100, and protease inhibitor cocktail (Complete, Roche)]. After incubation on a wheel for 2 h, unsolubilised material was removed by centrifugation for 15 min at 20,000*g*, and solubilised proteins were subjected to immunoprecipitations using anti-FLAG M2 affinity gel (Sigma-Aldrich). After 3 h of incubation on a wheel, the beads were washed twice with 1 mL buffer B and once with buffer C [10 mM Tris (pH 8.0), 100 mM NaCl, and 0.1% (wt/vol) Triton X-100]. Beads were air-dried, resuspended in Laemmli buffer, and subjected to SDS-PAGE and immunodetection with anti-FLAG antibodies and streptavidin coupled to alkaline phosphatase.

Bacterial two-hybrid assay

The adenylate cyclase-based bacterial two-hybrid technique [59] was used as previously published [24,60]. Briefly, pairs of proteins to be tested were fused to the isolated T18 and T25 catalytic domains of the *Bordetella* adelynate cyclase. After the transformation of the two plasmids producing the fusion proteins into the reporter BTH101 strain, plates were incubated at 30 °C for 48 h. Three independent colonies for each transformation were inoculated into 600 μL of LB medium supplemented with ampicillin, kanamycin, and IPTG (0.5 mM). After overnight growth at 30 °C, 10 μL of each culture was dropped onto LB supplemented with 40 μg/mL bromo-chloro-indolyl-β-D-galactopyrannoside (X-Gal) and was incubated for 16 h at 30 °C. The experiments were done at least in triplicate, and a representative result is shown.

Co-immunoprecipitation

100 mL of W3110 cells producing proteins of interest were grown to an OD600 of 0.4 and the expression of the cloned genes were induced with AHT or L-arabinose for 45 min. The cells were harvested, and the pellets were resuspended in 20 mM Tris–HCl (pH 8.0), 100 mM NaCl, 30% sucrose, 1 mM EDTA, 100 μg/mL lysozyme, 100 μg/mL DNase, and 100 μg/mL RNase supplemented with protease inhibitors (Complete, Roche) to an OD_{600} of 80 and were incubated on ice for 20 min. Cells were lysed by three passages at the French Press (800 psi), and lysates were clarified by centrifugation at 20,000*g* for 20 min. Supernatants were used for co-immunoprecipitation using anti-FLAG M2 affinity gel (Sigma-Aldrich). After 3 h of incubation, the beads were washed three times with 1 mL of 20 mM Tris–HCl (pH 8.0), 100 mM NaCl, and 15% sucrose, were resuspended in 25 μL of Laemmli loading buffer, boiled for 10 min, and subjected to SDS-PAGE and immunodetection analyses.

Fluorescence microscopy and statistical analyses

Overnight cultures of EAEC 17-2 derivative strains were diluted 1:100 in SIM medium and grown for 6 h to an OD_{600} of ~1.0 to maximise the expression of the *sci-1* T6SS gene cluster [55]. Cells were washed in phosphate-buffered saline (PBS), resuspended in PBS to an OD_{600} of ~50, and spotted on a thin pad of 1.5% agarose in PBS and covered with a cover slip. Microscopy recording and digital image processing have been performed as previously described [15,16,18,20,24]. The Z project (average intensity) plugin has been used to merge and flatten all Z-planes. Microscopy analyses were performed at least six times, each with technical triplicate, and a representative experiment is shown. The number of sheath per number of cells and sfGFP–TssF foci was measured manually.

Computer analyses

TMH predictions were made using HMMTop [61], TMHMM [62], TMpred [63], and PHDhtm [64]. Secondary structure predictions were made using the Psipred server†. Structural predictions and homology modelling of the tri-dimensional structure of $TssM_{Cyto/NTP}$ and $TssM_{Cyto/Ct}$ were performed using HHpred [39] or Swiss-Model [65], respectively. Figures were made using Chimera [66]. Amino acid sequences were aligned with T-COFFEE [67], and phylogenetic analyses were performed with phylogeny.fr [68].

Miscellaneous

SDS-PAGE was performed using standard protocols. For immunostaining, proteins were transferred onto nitrocellulose membranes, and immunoblots were probed with primary antibodies and goat secondary antibodies coupled to alkaline phosphatase and were developed in alkaline buffer in the presence of 5-bromo-4-chloro-3-indolylphosphate and nitro-blue tetrazolium. The anti-FLAG (M2 clone, Sigma-Aldrich), anti-VSV-G (clone P5D4, Sigma-Aldrich) monoclonal antibodies, the alkaline phosphatase-conjugated streptavidin (Pierce), and alkaline phosphatase-conjugated goat anti-mouse secondary antibodies (Beckman Coulter) have been purchased as indicated and used as recommended by the manufacturer.

Supplementary data to this article can be found online at http://dx.doi.org/10.1016/j.jmb.2016.08.032.

Acknowledgements

We thank the members of the Cascales, Lloubès, Cambillau, Sturgis, and Bouveret research groups for helpful discussions; Laure Journet for critical reading of the manuscript; Emmanuelle Bouveret and Julie Viala for advices and protocols for pKO3-dependent

chromosomal engineering; Abdlerahim Zoued for statistical analyses; Olivier Uderso, Isabelle Bringer, and Annick Brun for technical assistance; and Jimmy Switrumpey for encouragements. This work was supported by the Centre National de la Recherche Scientifique, the Aix-Marseille Université and the grants from the Agence Nationale de la Recherche to E.C. (ANR-10-JCJC-1303-03 and ANR-14-CE14-0006-02) and from the European Society of Clinical Microbiology and Infectious Diseases (ESCMID) to E.D. L.L. is supported by a doctoral fellowship from the French Ministry of Research and an end-of-thesis fellowship from the Fondation pour la Recherche Médicale (FDT20160435498). E.D. was supported by an EMBO short-term fellowship (ASTF-417-2015).

Received 1 August 2016;
Received in revised form 29 August 2016;
Accepted 30 August 2016
Available online xxxx

Keywords:
protein transport;
protein secretion;
type VI secretion;
bacterial competition;
membrane complex

Present address: M.-S. Aschtgen, Laboratoire des Sciences de l'Environnement Marin (LEMAR), Institut Universitaire Européen de la Mer (IUEM), Université de Bretagne Occidentale, CNRS, IRD, Ifremer – UMR 6539, Technopôle Brest Iroise, 29280 Plouzané, France; M. Guérin, Maquet Intervascular, 13600 La Ciotat, France.

†http://bioinf.cs.ucl.ac.uk/psipred/

Abbreviations used:
T6SS, type VI secretion system; BP, baseplate; MC, membrane complex; IM, inner membrane; OM, outer membrane; EAEC, enteroaggregative *Escherichia coli*; TMH, transmembrane helices; NTPase, nucleotide triphosphatase; NTP, nucleotide triphosphate; DPY-30, Dumpy-30; MPB, 3-(*N*-maleimidylpropionyl) biocytin; WT, wild-type; SIM, *sci-1*-inducing medium; AHT, anhydrotetracyclin; PBS, phosphate-buffered saline; spGFP, super folder Green Fluorescent Protein; DMSO, Diméthylsulfoxyde; GTP, Guanosine triphosphate.

References

[1] A.B. Russell, S.B. Peterson, J.D. Mougous, Type VI secretion system effectors: poisons with a purpose, Nat. Rev. Microbiol. 12 (2014) 137–148.
[2] E. Durand, C. Cambillau, E. Cascales, L. Journet, VgrG, Tae, Tle, and beyond: the versatile arsenal of type VI secretion effectors, Trends Microbiol. 22 (2014) 498–507.
[3] J. Alcoforado Diniz, Y.C. Liu, S.J. Coulthurst, Molecular weaponry: diverse effectors delivered by the type VI secretion system, Cell. Microbiol. 17 (2015) 1742–1751.
[4] A. Hachani, T.E. Wood, A. Filloux, Type VI secretion and anti-host effectors, Curr. Opin. Microbiol. 29 (2015) 81–93.
[5] G. Bönemann, A. Pietrosiuk, A. Mogk, Tubules and donuts: a type VI secretion story, Mol. Microbiol. 76 (2010) 815–821.
[6] E. Cascales, C. Cambillau, Structural biology of type VI secretion systems, Philos. Trans. R. Soc. Lond. Ser. B Biol. Sci. 367 (2012) 1102–1111.
[7] S.J. Coulthurst, The type VI secretion system—a widespread and versatile cell targeting system, Res. Microbiol. 164 (2013) 640–654.
[8] A. Zoued, Y.R. Brunet, E. Durand, M.S. Aschtgen, L. Logger, B. Douzi, L. Journet, C. Cambillau, E. Cascales, Architecture and assembly of the type VI secretion system, Biochim. Biophys. Acta 1843 (2014) 1664–1673.
[9] S. Kube, P. Wendler, Structural comparison of contractile nanomachines, AIMS Biophys. 2 (2015) 88–115.
[10] M. Basler, Type VI secretion system: secretion by a contractile nanomachine, Philos. Trans. R. Soc. Lond. Ser. B Biol. Sci. 370 (2015) 1679.
[11] B.T. Ho, T.G. Dong, J.J. Mekalanos, A view to a kill: the bacterial type VI secretion system, Cell Host Microbe 15 (2014) 9–21.
[12] F.R. Cianfanelli, L. Monlezun, S.J. Coulthurst, Aim, load, fire: the type VI secretion system, a bacterial nanoweapon, Trends Microbiol. 24 (2016) 51–62.
[13] P.G. Leiman, M. Basler, U.A. Ramagopal, J.B. Bonanno, J.M. Sauder, S. Pukatzki, S.K. Burley, S.C. Almo, J.J. Mekalanos, Type VI secretion apparatus and phage tail-associated protein complexes share a common evolutionary origin, Proc. Natl. Acad. Sci. U. S. A. 106 (2009) 4154–4159.
[14] M. Basler, M. Pilhofer, G.P. Henderson, G.J. Jensen, J.J. Mekalanos, Type VI secretion requires a dynamic contractile phage tail-like structure, Nature 483 (2012) 182–186.
[15] Y.R. Brunet, A. Zoued, F. Boyer, B. Douzi, E. Cascales, The type VI secretion TssEFGK-VgrG phage-like baseplate is recruited to the TssJLM membrane complex via multiple contacts and serves as assembly platform for tail tube/sheath polymerization, PLoS Genet. 15 (3) (2015) e1005545, 315–321.
[16] E. Durand, V.S. Nguyen, A. Zoued, L. Logger, G. Péhau-Arnaudet, M.S. Aschtgen, S. Spinelli, A. Desmyter, B. Bardiaux, A. Dujeancourt, A. Roussel, C. Cambillau, E. Cascales, R. Fronzes, Biogenesis and structure of a type VI secretion membrane core complex, Nature 523 (2015) 555–560.
[17] E.R. Ballister, A.H. Lai, R.N. Zuckermann, Y. Cheng, J.D. Mougous, *In vitro* self-assembly of tailorable nanotubes from a simple protein building block, Proc. Natl. Acad. Sci. U. S. A. 105 (2008) 3733–3738.
[18] Y.R. Brunet, J. Hénin, H. Celia, E. Cascales, Type VI secretion and bacteriophage tail tubes share a common assembly pathway, EMBO Rep. 15 (2014) 315–321.
[19] M. Kudryashev, R.Y. Wang, M. Brackmann, S. Scherer, T. Maier, D. Baker, F. DiMaio, H. Stahlberg, E.H. Egelman, M. Basler, Structure of the type VI secretion system contractile sheath, Cell 160 (2015) 952–962.
[20] Y.R. Brunet, L. Espinosa, S. Harchouni, T. Mignot, E. Cascales, Imaging type VI secretion-mediated bacterial killing, Cell Rep. 3 (2013) 36–41.
[21] M. Basler, B.T. Ho, J.J. Mekalanos, Tit-for-tat: type VI secretion system counterattack during bacterial cell–cell interactions, Cell 152 (2013) 884–894.

Please cite this article as: L. Logger, et al., Molecular Dissection of the Interface between the Type VI Secretion TssM Cytoplasmic Domain and the TssG Baseplate Component, J. Mol. Biol. (2016), http://dx.doi.org/10.1016/j.jmb.2016.08.032

[22] A. Zoued, E. Durand, Y.R. Brunet, S. Spinelli, B. Douzi, M. Guzzo, N. Flaugnatti, P. Legrand, L. Journet, R. Fronzes, T. Mignot, C. Cambillau, E. Cascales, Priming and polymerization of a bacterial contractile tail structure, Nature 531 (2016) 59–63.
[23] S. Pukatzki, A.T. Ma, A.T. Revel, D. Sturtevant, J.J. Mekalanos, Type VI secretion system translocates a phage tail spike-like protein into target cells where it cross-links actin, Proc. Natl. Acad. Sci. U. S. A. 104 (2007) 15,508–15,513.
[24] A. Zoued, E. Durand, C. Bebeacua, Y.R. Brunet, B. Douzi, C. Cambillau, E. Cascales, L. Journet, TssK is a trimeric cytoplasmic protein interacting with components of both phage-like and membrane anchoring complexes of the type VI secretion system, J. Biol. Chem. 288 (2013) 27,031–27,041.
[25] G. English, O. Byron, F.R. Cianfanelli, A.R. Prescott, S.J. Coulthurst, Biochemical analysis of TssK, a core component of the bacterial type VI secretion system, reveals distinct oligomeric states of TssK and identifies a TssK–TssFG subcomplex, Biochem. J. 461 (2014) 291–304.
[26] N.M. Taylor, N.S. Prokhorov, R.C. Guerrero-Ferreira, M.M. Shneider, C. Browning, K.N. Goldie, H. Stahlberg, P.G. Leiman, Structure of the T4 baseplate and its function in triggering sheath contraction, Nature 533 (2016) 346–352.
[27] S. Planamente, O. Salih, E. Manoli, D. Albesa-Jové, P.S. Freemont, A. Filloux, TssA forms a gp6-like ring attached to the type VI secretion sheath, EMBO J. 35 (15) (Aug 1 2016) 1613–1627, http://dx.doi.org/10.15252/embj.201694024 (Epub 2016 Jun 10).
[28] M.S. Aschtgen, C.S. Bernard, S. De Bentzmann, R. Lloubès, E. Cascales, SciN is an outer membrane lipoprotein required for type VI secretion in enteroaggregative *Escherichia coli*, J. Bacteriol. 190 (2008) 7523–7531.
[29] L.S. Ma, J.S. Lin, E.M. Lai, An IcmF family protein, ImpLM, is an integral inner membrane protein interacting with ImpKL, and its walker a motif is required for type VI secretion system-mediated hcp secretion in *Agrobacterium tumefaciens*, J. Bacteriol. 191 (2009) 4316–4129.
[30] M.S. Aschtgen, M. Gavioli, A. Dessen, R. Lloubès, E. Cascales, The SciZ protein anchors the enteroaggregative *Escherichia coli* type VI secretion system to the cell wall, Mol. Microbiol. 75 (2010) 886–899.
[31] M.S. Aschtgen, A. Zoued, R. Lloubès, L. Journet, E. Cascales, The C-tail anchored TssL subunit, an essential protein of the enteroaggregative *Escherichia coli* Sci-1 type VI secretion system, is inserted by YidC, Microbiologyopen 1 (2012) 71–82.
[32] E. Durand, A. Zoued, S. Spinelli, P.J. Watson, M.S. Aschtgen, L. Journet, C. Cambillau, E. Cascales, Structural characterization and oligomerization of the TssL protein, a component shared by bacterial type VI and type IVb secretion systems, J. Biol. Chem. 287 (2012) 14,157–14,168.
[33] J. Zheng, K.Y. Leung, Dissection of a type VI secretion system in *Edwardsiella tarda*, Mol. Microbiol. 66 (2007) 1192–1206.
[34] C. Felisberto-Rodrigues, E. Durand, M.S. Aschtgen, S. Blangy, M. Ortiz-Lombardia, B. Douzi, C. Cambillau, E. Cascales, Towards a structural comprehension of bacterial type VI secretion systems: characterization of the TssJ–TssM complex of an *Escherichia coli* pathovar, PLoS One. 10 (3) (Mar 26 2015) e0122187.
[35] V.S. Nguyen, L. Logger, S. Spinelli, A. Desmyter, T.T. Le, C. Kellenberger, B. Douzi, E. Durand, A. Roussel, E. Cascales, C. Cambillau, Inhibition of type VI secretion by an anti-TssM llama nanobody, PLoS One 10 (3) (Mar 26 2015) e0122187.
[36] A.J. Gerc, A. Diepold, K. Trunk, M. Porter, C. Rickman, J.P. Armitage, N.R. Stanley-Wall, S.J. Coulthurst, Visualization of the Serratia type VI secretion system reveals unprovoked attacks and dynamic assembly, Cell Rep. 12 (2015) 2131–2142.
[37] L.S. Ma, F. Narberhaus, E.M. Lai, IcmF family protein TssM exhibits ATPase activity and energizes type VI secretion, J. Biol. Chem. 287 (2012) 15,610–15,621.
[38] M. Bogdanov, W. Zhang, J. Xie, W. Dowhan, Transmembrane protein topology mapping by the substituted cysteine accessibility method (SCAM(TM)): application to lipid-specific membrane protein topogenesis, Methods 36 (2005) 148–171.
[39] J. Söding, A. Biegert, A.N. Lupas, The HHpred interactive server for protein homology detection and structure prediction, Nucleic Acids Res. 33 (2005) W244–W248.
[40] L. Baugh, L.A. Gallagher, R. Patrapuvich, M.C. Clifton, A.S. Gardberg, T.E. Edwards, B. Armour, D.W. Begley, S.H. Dieterich, D.M. Dranow, J. Abendroth, J.W. Fairman, D. Fox III, B.L. Staker, I. Phan, A. Gillespie, R. Choi, S. Nakazawa-Hewitt, M.T. Nguyen, A. Napuli, L. Barrett, G.W. Buchko, R. Stacy, P.J. Myler, L.J. Stewart, C. Manoil, W.C. Van Voorhis, Combining functional and structural genomics to sample the essential *Burkholderia* structome, PLoS One 8 (1) (2013) e53851, http://dx.doi.org/10.1371/journal.pone.0053851 (Epub 2013 Jan 31).
[41] I. Hanukoglu, Rossmann fold: a beta-alpha-beta fold at dinucleotide binding sites, Biochem. Mol. Biol. Educ. 43 (2015) 206–209.
[42] X. Wang, Z. Lou, X. Dong, W. Yang, Y. Peng, B. Yin, Y. Gong, J. Yuan, W. Zhou, M. Bartlam, X. Peng, Z. Rao, Crystal structure of the C-terminal domain of human DPY-30-like protein: a component of the histone methyltransferase complex, J. Mol. Biol. 390 (2009) 530–537.
[43] N. Flaugnatti, T.T. Le, S. Canaan, M.S. Aschtgen, V.S. Nguyen, S. Blangy, C. Kellenberger, A. Roussel, C. Cambillau, E. Cascales, L. Journet, A phospholipase A1 anti-bacterial T6SS effector interacts directly with the C-terminal domain of the VgrG spike protein for delivery, Mol. Microbiol. 99 (2016) 1099–1118.
[44] V. Tremblay, P. Zhang, C.P. Chaturvedi, J. Thornton, J.S. Brunzelle, G. Skiniotis, A. Shilatifard, M. Brand, J.F. Couture, Molecular basis for DPY-30 association to COMPASS-like and NURF complexes, Structure 22 (2014) 1821–1830.
[45] V.A. Kostyuchenko, P.G. Leiman, P.R. Chipman, S. Kanamaru, M.J. van Raaij, F. Arisaka, V.V. Mesyanzhinov, M.G. Rossmann, Three-dimensional structure of bacteriophage T4 baseplate, Nat. Struct. Biol. 10 (2003) 688–693.
[46] V.A. Kostyuchenko, P.R. Chipman, P.G. Leiman, F. Arisaka, V.V. Mesyanzhinov, M.G. Rossmann, The tail structure of bacteriophage T4 and its mechanism of contraction, Nat. Struct. Mol. Biol. 12 (2005) 810–813.
[47] P.G. Leiman, F. Arisaka, M.J. van Raaij, V.A. Kostyuchenko, A.A. Aksyuk, S. Kanamaru, M.G. Rossmann, Morphogenesis of the T4 tail and tail fibers, Virol. J. 7 (2010) 355.
[48] A. Paschos, A. den Hartigh, M.A. Smith, V.L. Atluri, D. Sivanesan, R.M. Tsolis, C. Baron, An *in vivo* high-throughput screening approach targeting the type IV secretion system component VirB8 identified inhibitors of *Brucella* abortus 2308 proliferation, Infect. Immun. 79 (2011) 1033–1043.
[49] M.A. Smith, M. Coinçon, A. Paschos, B. Jolicoeur, P. Lavallée, J. Sygusch, C. Baron, Identification of the binding site of *Brucella* VirB8 interaction inhibitors, Chem. Biol. 19 (2012) 1041–1048.
[50] A. Zaslaver, A. Bren, M. Ronen, S. Itzkovitz, I. Kikoin, S. Shavit, W. Liebermeister, M.G. Surette, U. Alon, A comprehensive library of fluorescent transcriptional reporters for *Escherichia coli*, Nat. Methods 3 (2006) 623–628.

Please cite this article as: L. Logger, et al., Molecular Dissection of the Interface between the Type VI Secretion TssM Cytoplasmic Domain and the TssG Baseplate Component, J. Mol. Biol. (2016), http://dx.doi.org/10.1016/j.jmb.2016.08.032

[51] K.A. Datsenko, B.L. Wanner, One-step inactivation of chromosomal genes in *Escherichia coli* K-12 using PCR products, Proc. Natl. Acad. Sci. U. S. A. 97 (2000) 6640–6645.
[52] M.K. Chaveroche, J.M. Ghigo, C. d'Enfert, A rapid method for efficient gene replacement in the filamentous fungus *Aspergillus nidulans*, Nucleic Acids Res. 28 (2000) E97.
[53] A.J. Link, D. Phillips, G.M. Church, Methods for generating precise deletions and insertions in the genome of wild-type *Escherichia coli*: application to open reading frame characterization, J. Bacteriol. 179 (1997) 6228–6237.
[54] A. Battesti, E. Bouveret, Acyl carrier protein/SpoT interaction, the switch linking SpoT-dependent stress response to fatty acid metabolism, Mol. Microbiol. 62 (2006) 1048–1063.
[55] Y.R. Brunet, C.S. Bernard, M. Gavioli, R. Lloubès, E. Cascales, An epigenetic switch involving overlapping fur and DNA methylation optimizes expression of a type VI secretion gene cluster, PLoS Genet. 7 (7) (Jul 2011) e1002205, http://dx.doi.org/10.1371/journal.pgen.1002205 (Epub 2011 Jul 28).
[56] F. van den Ent, J. Löwe, RF cloning: a restriction-free method for inserting target genes into plasmids, J. Biochem. Biophys. Methods 67 (2006) 67–74.
[57] S.J. Jakubowski, V. Krishnamoorthy, E. Cascales, P.J. Christie, *Agrobacterium tumefaciens* VirB6 domains direct the ordered export of a DNA substrate through a type IV secretion system, J. Mol. Biol. 341 (2004) 961–977.
[58] E.L. Goemaere, A. Devert, R. Lloubès, E. Cascales, Movements of the TolR C-terminal domain depend on TolQR ionizable key residues and regulate activity of the Tol complex, J. Biol. Chem. 282 (2007) 17,749–17,757.
[59] G. Karimova, J. Pidoux, A. Ullmann, D. Ladant, A bacterial two-hybrid system based on a reconstituted signal transduction pathway, Proc. Natl. Acad. Sci. U. S. A. 95 (1998) 5752–5756.
[60] A. Battesti, E. Bouveret, The bacterial two-hybrid system based on adenylate cyclase reconstitution in *Escherichia coli*, Methods 58 (2012) 325–334.
[61] G.E. Tusnády, I. Simon, Principles governing amino acid composition of integral membrane proteins: application to topology prediction, J. Mol. Biol. 283 (1998) 489–506.
[62] A. Krogh, B. Larsson, G. von Heijne, E.L. Sonnhammer, Predicting transmembrane protein topology with a hidden Markov model: application to complete genomes, J. Mol. Biol. 305 (2001) 567–580.
[63] K. Hofmann, W. Stoffel, A database of membrane spanning protein segments, Biol. Chem. 374 (1993) 166.
[64] B. Rost, P. Fariselli, R. Casadio, Topology prediction for helical transmembrane proteins at 86% accuracy, Protein Sci. 5 (1996) 1704–1718.
[65] M. Biasini, S. Bienert, A. Waterhouse, K. Arnold, G. Studer, T. Schmidt, F. Kiefer, T. Gallo Cassarino, M. Bertoni, L. Bordoli, T. Schwede, SWISS-MODEL: modelling protein tertiary and quaternary structure using evolutionary information, Nucleic Acids Res. 42 (2014) W252–W258.
[66] E.F. Pettersen, T.D. Goddard, C.C. Huang, G.S. Couch, D.M. Greenblatt, E.C. Meng, T.E. Ferrin, UCSF chimera–a visualization system for exploratory research and analysis, J. Comput. Chem. 25 (2004) 1605–1612.
[67] P. Di Tommaso, S. Moretti, I. Xenarios, M. Orobitg, A. Montanyola, J.M. Chang, J.F. Taly, C. Notredame, T-coffee: a web server for the multiple sequence alignment of protein and RNA sequences using structural information and homology extension, Nucleic Acids Res. 39 (2011) W13–W17.
[68] A. Dereeper, V. Guignon, G. Blanc, S. Audic, S. Buffet, F. Chevenet, J.F. Dufayard, S. Guindon, V. Lefort, M. Lescot, J.M. Claverie, O. Gascuel, Phylogeny.fr: robust phylogenetic analysis for the non-specialist, Nucleic Acids Res. 36 (2008) W465–W469.
[69] A. Zoued, C.J. Cassaro, E. Durand, B. Douzi, A.P. España, C. Cambillau, L. Journet, E. Cascales, Structure–function analysis of the TssL cytoplasmic domain reveals a new interaction between the type VI secretion baseplate and membrane complexes, J. Mol. Biol. (2016), http://dx.doi.org/10.1016/j.jmb.2016.08.030.

Please cite this article as: L. Logger, et al., Molecular Dissection of the Interface between the Type VI Secretion TssM Cytoplasmic Domain and the TssG Baseplate Component, J. Mol. Biol. (2016), http://dx.doi.org/10.1016/j.jmb.2016.08.032